



HAL
open science

Port-Hamiltonian modeling and control of a curling HASEL actuator

Nelson Cisneros, Yongxin Wu, Kanty Rabenorosoa, Yann Le Gorrec

► **To cite this version:**

Nelson Cisneros, Yongxin Wu, Kanty Rabenorosoa, Yann Le Gorrec. Port-Hamiltonian modeling and control of a curling HASEL actuator. 8th IFAC Workshop on Lagrangian and Hamiltonian Methods for Non Linear Control, Jun 2024, Besançon, France. hal-04432915

HAL Id: hal-04432915

<https://hal.science/hal-04432915>

Submitted on 15 Feb 2024

HAL is a multi-disciplinary open access archive for the deposit and dissemination of scientific research documents, whether they are published or not. The documents may come from teaching and research institutions in France or abroad, or from public or private research centers.

L'archive ouverte pluridisciplinaire **HAL**, est destinée au dépôt et à la diffusion de documents scientifiques de niveau recherche, publiés ou non, émanant des établissements d'enseignement et de recherche français ou étrangers, des laboratoires publics ou privés.

Port-Hamiltonian modeling and control of a curling HASEL actuator[★]

Nelson Cisneros, Yongxin Wu, Kanty Rabenorosoa,
Yann Le Gorrec

*FEMTO-ST institute, UBFC, CNRS, Besançon, France. (emails:
nelson.cisneros@femto-st.fr, yongxin.wu@femto-st.fr,
rkanty@femto-st.fr, yann.le.gorrec@femto-st.fr)*

Abstract: This paper is concerned with the modeling and control of a curling Hydraulically Amplified Self-healing Electrostatic (HASEL) actuator using the port-Hamiltonian (PH) approach. For that purpose, we use a modular approach and consider the HASEL actuator as an interconnection of elementary subsystems. Each subsystem is modeled by an electrical component consisting of a capacitor in parallel with an inductor connected through the conservation of volume of the moving liquid to a mechanical structure based on inertia, linear, and torsional springs. The parameters are then identified, and the model is validated on the experimental setup. Position control is achieved by using Interconnection and Damping Assignment-Passivity Based Control (IDA-PBC) with integral action (IA) for disturbance rejection. Simulation results show the efficiency of the proposed controller.

Keywords: Soft actuator, HASEL actuator, Port-Hamiltonian systems, IDA-PBC design.

1. INTRODUCTION

In recent years, one of the most interesting technologies that have been developed for soft robotic applications is the Hydraulically Amplified Self-healing Electrostatic (HASEL) actuator (Acome et al., 2018).

HASEL actuators blend the advantages of Dielectric Elastomer Actuators (DEAs) and fluid-driven soft actuators, combining the convenience of electrical control, excellent electromechanical performances, extensive design flexibility, and various actuation modes (Rothmund et al., 2021). There are different types of HASEL actuators, such as peano, planar, elastomeric donut, quadrant donut, high-strain peano, and curling actuators. Some interesting applications of HASEL actuators can be found in the literature: a soft gripper for aerial object manipulation (Kim and Cha, 2021), an actuator powering a robotic arm (Acome et al., 2018), an electro-hydraulic rolling soft wheel (Ly et al., 2022), a peano actuator for enhanced strain, load, and rotary motion (Tian et al., 2022) and soft-actuated joints based on the hydraulic mechanism used in spider legs (Kellaris et al., 2021).

In this paper, we consider, as a benchmark the design, modeling, and control of a simple curling HASEL actuator that can be used as a basic element in more complex robotic structures such as robotic hands or soft grippers. The considered curling HASEL actuator is based on a strain limiting layer that is added to the traditional HASEL mechanism (Acome et al., 2018) to change its motion from linear to angular deformation (Rothmund et al., 2021). It is important to derive a reliable model representing the system's dynamics to control the actuator. Many

papers dealing with the modeling of HASEL actuators have been recently proposed in the literature. In (Volchko et al., 2022), Dynamic Mode Decomposition with Control (DMDc) is applied to derive a linear model, approximating the system's dynamics. In (Hainsworth et al., 2022), a non-linear reduced-order mass-spring-damper (MSD) model for a linear HASEL actuator is proposed. However, these works do not take into account the non-linear behavior (such as the drift effect) or electrical dynamics of HASEL actuators in the model, which can make the control design more challenging and difficult to implement in a real-world application.

Port-Hamiltonian (PH) formulations are particularly well adapted to represent multi-physical systems. The PH approach is then an excellent candidate to represent the considered dynamics of the HASEL actuator. Interconnection and Damping Assignment-Passivity Based Control (IDA-PBC) serves as a highly effective tool for generating asymptotically stabilizing controllers for Port-Controlled Hamiltonian (PCH) models. (Ortega et al., 2002). Previous works used PHS to model soft robots with energy shaping and IDA-PBC controllers, showing good results. In (Franco et al., 2021b) and (Franco et al., 2021a), energy shaping controllers are used to control the position of a soft continuum manipulator with a large number of degrees of freedom (DOF). In (Ayala et al., 2022), the IDA-PBC method has been successfully used to control a nonlinear Cosserat rod model using an early lumping approach. More recently, in (Yeh et al., 2022), a PH formulation of a one DOF of HASEL planar actuator with position control using an IDA-PBC with Integral Action (IA) has been proposed. Compare to (Yeh et al., 2022) we consider here an actuator with bending motion instead of linear deformation. This introduces nonlinearities in the

[★] This work is supported by the EIPHI Graduate School (contract ANR-17-EURE-0002).

interconnection matrix. Furthermore, we aim to capture the end position drift effect. The main contributions of this paper are:

- We modeled a curling HASEL actuator using the port-Hamiltonian approach to capture the actuator's electrical and mechanical dynamics.
- We identified the model compared with experimental data and validated it with different input voltages.
- We designed an IDA-PBC controller with integral action to control the end point position of the curling HASEL actuator and reject the input disturbances.

This paper is organized as follows: Section 2 presents the experimental setup of the curling HASEL actuator and its modeling under the PH framework. The parameter identification is detailed in Section 3. In Section 4, the controller design is presented. Section 5 presents the simulation results, and the conclusions are given in Section 6.

2. CURLING HASEL ACTUATOR AND ITS PH MODELING

In this section, we first introduce the experimental curling HASEL actuator that is used as a benchmark. We describe the setup and its working principle with reasonable hypotheses that will be used for modeling purposes. We then derive the PH model for this actuator.

2.1 Experimental setup

The experimental setup is shown in Fig. 1. To measure the position, we use a profile laser sensor, Keyence LJ-V7080. We use the high voltage amplifier Trek model 610E. The HASEL actuator used in this work comes from *Artimus Robotics*. We use a dSPACE card CLP1104 to receive and send signals from/to the laser position sensor and high voltage amplifier. The pictures of Fig. 1 (right) show

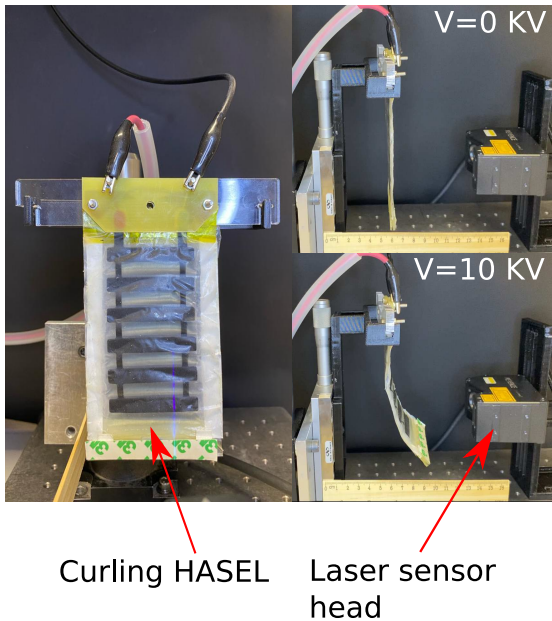


Fig. 1. Experimental setup laser sensor and curling HASEL.

the deformation of the actuator without (upper figure) and with an applied voltage (lower figure). Applying high voltage, the actuator can achieve a horizontal displacement of approximately 3 cm.

2.2 Curling HASEL actuator description and hypothesis

The curling HASEL actuator consists of a polymer shell filled with dielectric liquid and half covered by a pair of electrodes attached to a strain-limiting layer to get the bending motion. When an electric field is applied to the electrodes, it creates Maxwell stress acting on the shell that pushes the dielectric liquid inside the shell. This hydraulic pressure changes the shape of the shell and, from the strain-limiting layer, induces the bending of the actuator (Rothmund et al., 2021).

We consider that the actuator depth is uniform, so we proceed to a two-dimensional analysis. We model the actuator using interconnected subsystems. We separate each subsystem model into a chamber and a shell (cf Fig. 2).

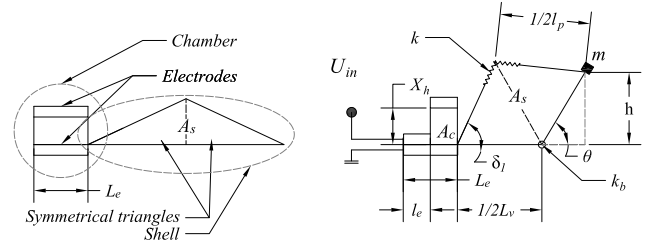


Fig. 2. Basic subsystem. Left: electrodes are totally unzipped. Right: Electrodes are partially zipped when voltage is applied. The shell is deformed.

The chamber is the area between the electrodes whilst the shell receives the dielectric liquid when the electrodes are zipped. The total volume (the shell's volume plus the chamber's volume) is considered constant, and the dielectric liquid is incompressible. The bending of the bottom film is modeled as a torsional spring. The top film of the shell is considered to be elongable and contains mechanical energy. The elongation is modeled as a linear spring. The shell will take on a specific shape based on the volume transferred from the chamber to the shell, resulting from the zipping of the electrodes, which takes place when high voltage is applied. The electrodes are modeled as a variable capacitor. The model considers a variable length of the zipped electrodes. The distance between the unzipped electrodes part is considered constant, see Fig. 2.

2.3 Geometric relations

In this part, we present the relations existing between the angle θ and the length of the zipped electrodes l_e . Then, we derive the actuator position $h(\theta)$ from θ , i.e., the displacement of the end position of the actuator.

It is crucial to obtain a relation between θ and l_e because the electrode's capacitance depends on l_e . Therefore, it allows us to relate the electrical charge, that depends on the capacitance, with the derivative of the electrical

energy respecting the angle θ , joining the electrical and the mechanical part.

We represent the chamber as a rectangular area and the shell is modeled as two symmetric triangles. Fig. 2 shows the model variables of a basic subsystem.

The area inside the shell is equal to:

$$A_s = \frac{1}{4} l_p L_v \sin(\delta_1) \quad (1)$$

with

$$\delta_1 = \frac{\pi + \theta}{2} - \sin^{-1} \left(\frac{L_v}{l_p} \sin \left(\frac{\pi - \theta}{2} \right) \right). \quad (2)$$

The total area is:

$$A_T = A_s + X_h(L_e - l_e), \quad (3)$$

where L_v and l_p are the lengths of the bottom and the top film. X_h is the height of the chamber and L_e is the length of the chamber.

The zipped electrodes length is then:

$$l_e = L_e - \frac{1}{X_h} \left(A_T - \frac{L_v l_p}{4} \sin(\delta_1) \right). \quad (4)$$

2.4 Curling HASEL port-Hamiltonian model

This section presents the port-Hamiltonian model for the curling HASEL actuator. PH formulations consist in using the energy variables as state variables and in writing the dynamics of the system on the form (van der Schaft, 2000):

$$\begin{aligned} \dot{x} &= [J(x) - R(x)] \frac{\partial H}{\partial x}(x) + g(x)u; \\ y &= g^T(x) \frac{\partial H}{\partial x}(x), \end{aligned} \quad (5)$$

where $J(x) = -J^T(x)$ is the interconnection matrix, $R(x) = R^T(x) \geq 0$ is the dissipation matrix and H is the total energy of the system (Hamiltonian).

By combining basic subsystems, we can represent the overall dynamic behavior of the HASEL actuator. In what follows we consider four subsystems (cf Fig. 3) but the model can be extended to $n \in \mathbb{N}$ subsystems. We consider that the subsystems share the same input voltage. The total energy of the system is given by:

$$H(\theta, l_p, p, \phi, Q) = H_\theta(\theta) + H_{l_p}(l_p) + H_g(\theta) + H_p(p) + H_\phi(\phi, Q) + H_Q(Q, \phi, \theta, l_p), \quad (6)$$

where

$$H_\theta = \frac{1}{2} \sum_{i=1}^n K_{b_i} \theta_i^2 = \frac{1}{2} \theta^T K_b \theta \quad (7)$$

is the potential energy where $K_b = \text{diag}[K_{b_1} K_{b_2} \dots K_{b_n}]$ is the stiffness matrix and $\theta = [\theta_1 \theta_2 \dots \theta_n]$ represents the angular vector of each subsystem, the second term is the potential energy related to the linear springs:

$$H_{l_p} = \frac{1}{4} \sum_{i=1}^n K_i (l_{p_i} - L_{p_i})^2 = \frac{1}{4} (l_p - L_p)^T K (l_p - L_p), \quad (8)$$

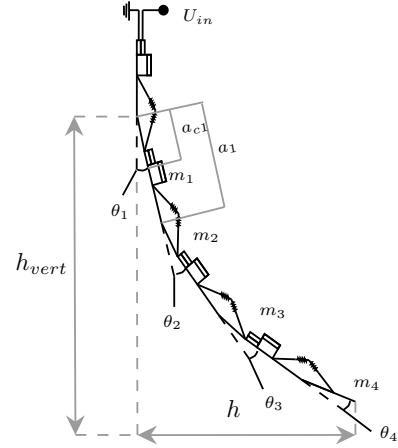


Fig. 3. Four interconnected subsystems. The same voltage is applied to the entire system.

where $K = \text{diag}[K_1 K_2 \dots K_n]$ and $l_p^T = [l_{p_1} l_{p_2} \dots l_{p_n}]$, the third term is the total potential energy related to gravity:

$$H_g = \sum_{i=1}^n H_{g_i}, \quad (9)$$

and the fourth term the kinetic energy:

$$H_p = \frac{1}{2} p^T M^{-1} p, \quad (10)$$

where M is the matrix of inertia and p is the vector of angular momentum $p^T = [p_1 p_2 \dots p_n]$.

The electrical energy has two components: the energy related to the magnetic flux that allows us to represent the drift effect and the energy related to the charge. The inductor discharges the capacitor over time.

$$H_\phi = \frac{1}{2} \sum_{i=1}^n \frac{\phi_i^2}{L_i} = \frac{1}{2} \phi^T L^{-1} \phi \quad (11)$$

The energy stored in the capacitor is:

$$H_Q = \frac{1}{2} \sum_{i=1}^n \frac{Q_i^2}{C_{s_i}} = \frac{1}{2} Q^T C^{-1} Q, \quad (12)$$

where $\phi^T = [\phi_1 \phi_2 \dots \phi_n]$ is the magnetic flux, L is the inductance of the equivalent electric circuit $L = \text{diag}[L_1 L_2 \dots L_n]$. $C = \text{diag}[C_{s_1} C_{s_2} \dots C_{s_n}]$ is the capacitance of the equivalent electric circuit and $Q = [Q_1 Q_2 \dots Q_n]^T$ is the charge. The capacitance of a subsystem is $C_{s_i} = C_{1_i} + C_{2_i}$ where $C_{1_i} = \frac{\epsilon_0 \epsilon_r w l_{e_i}}{2t}$ is the capacitance of the zipped part and $C_{2_i} = \frac{\epsilon_0 \epsilon_r w (L_e - l_{e_i})}{2t + X_h}$ the capacitance of the unzipped part.

The input gain is $ga^T = [ga_1 ga_2 \dots ga_n]$. To capture the system's nonlinearities, the input gain is a nonlinear function that depends on the angular position $ga_i = \gamma_1 \cos(\gamma_2 \theta_i)$.

The conductance of the equivalent electric circuit is $\bar{R} = \text{diag}[\frac{1}{\bar{R}_1} \frac{1}{\bar{R}_2} \dots \frac{1}{\bar{R}_n}]$. The damping coefficient of the system is $b = \text{diag}[b_1 b_2 \dots b_n]$. The resistance associated to the inductance is $r_L = \text{diag}[r_{L_1} r_{L_2} \dots r_{L_n}]$. We define

the term $d = \text{diag}\left(\frac{2A_s}{l_p}\right)$. The proposed port-Hamiltonian model of the curling HASEL actuator is then:

$$\underbrace{\begin{bmatrix} \dot{\theta} \\ \dot{l}_p \\ \dot{p} \\ \dot{\phi} \\ \dot{Q} \end{bmatrix}}_{\dot{x}} = \underbrace{\begin{bmatrix} 0 & 0 & I & 0 & 0 \\ 0 & 0 & d & 0 & 0 \\ -I & -d & -b & 0 & 0 \\ 0 & 0 & 0 & -r_L & I \\ 0 & 0 & 0 & -I & -\bar{R} \end{bmatrix}}_{J-R} \underbrace{\begin{bmatrix} \nabla_{\theta} H \\ \nabla_{l_p} H \\ \nabla_p H \\ \nabla_{\phi} H \\ \nabla_Q H \end{bmatrix}}_{\nabla_x H} + \underbrace{\begin{bmatrix} 0 \\ 0 \\ 0 \\ 0 \\ \bar{R}ga(\theta) \end{bmatrix}}_g U_{in}; \quad (13)$$

$$y = \underbrace{(\bar{R}ga(\theta))^T C^{-1} Q}_{g^T \nabla_x H}.$$

The output $y = i_e$ is the current that is power-conjugated to the input voltage. The energy balance equation can be written as:

$$\begin{aligned} \frac{\partial H}{\partial t} &= -\frac{\partial H^T}{\partial x} R \frac{\partial H}{\partial x} + y^T u; \\ \frac{\partial H}{\partial t} &\leq y^T u = i_e U_{in}. \end{aligned} \quad (14)$$

The displacement for n interconnected subsystems is computed as

$$h(\theta) = (L_v + L_e) \left(\sum_{i=1}^n \sin\left(\sum_{j=1}^i \theta_j\right) \right) \quad (15)$$

3. MODEL IDENTIFICATION AND VALIDATION

We identify the key parameters of the system using the experimental data obtained from the experimental setup of Fig. 2.1. The Levenberg–Marquardt algorithm is used to find the parameters K_b , b , L , γ_1 and γ_2 . The identification results are shown in Fig. 4 with a fitting of 90.7%. Two datasets are used to validate the obtained parameters, one with negative inputs and another with positive inputs, as shown in Fig. 5.

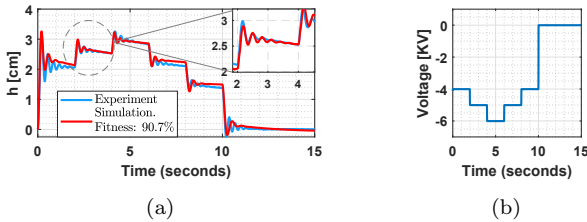


Fig. 4. (4a) Model identification, fitness: 90.7%. (4b) Input signal.

The fitting between the model and the experimental data is computed using the normalized root mean squared error (NRMSE):

$$fit(i) = \frac{\|x_{ref}(\cdot) - x_{data}(\cdot)\|}{\|x_{ref}(\cdot) - (x_{ref}(\cdot))\|} \quad (16)$$

where $\|\cdot\|$ is the 2-norm of a vector.

One can see the identified model can cope with the main dynamics of the considered Curling HASEL actuator with a fitting comprised between 85% and 89.33%. The identified parameters are listed in Table 1.

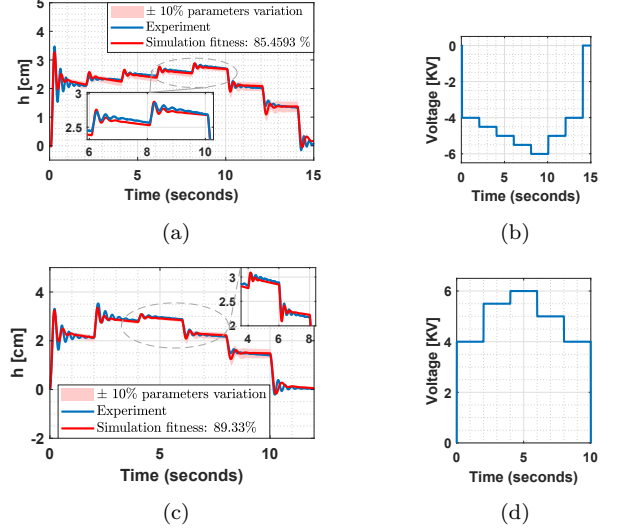


Fig. 5. (5a) Model validation, negative input fitness: 85.46% (5b) Input signal. 5c) Model validation, positive input fitness: 89.33% (5d) Positive input signal. We can observe the model's behavior in response to a variation of 10% around the nominal values.

Symbol	Value	Units	Definition
L_p	0.015	m	Length of top film
L_v	0.015	m	Length of bottom film
L_e	0.015	m	Length of electrodes
X_h	0.002	m	Chamber high
m	0.047	kg	Mass
ϵ_r	2.2	F/m	Relative permittivity
ϵ_0	8.854×10^{-12}	F/m	Vacuum permittivity
w	0.05	m	Actuator width
t	18×10^{-6}	m	Film thickness
R_i	10	Ω	Resistance
r_L	20	Ω	Resistance
L	150	F	Inductance
K	400	N/m	Spring constant
K_b	0.202	Nm/rad	Torsional spring constant
b	0.0199	kgs	Damping
γ_1	104.33	-	Gain parameter
γ_2	7.67	-	Gain parameter

Table 1. Model parameters.

4. POSITION CONTROL DESIGN

In this work, we aim to control the endpoint position of the curling HASEL actuator (denoted by h). To this end, we propose an IDA-PBC design method. This method aims to find a state feedback control law $\beta(x)$ to map the open-loop system to a desired closed-loop system of the form:

$$\dot{x} = (J_d - R_d) \nabla_x H_d \quad (17)$$

with the desired interconnection and damping matrices J_d , R_d and the desired energy function H_d in the closed-loop system. The control scheme is shown in Fig. 6.

The desired equilibrium points $x^* = [\theta^*, l_p^*, 0, \phi^*, Q^*]^T$ which can be computed from the desired endpoint position h^* (solving (15)) and the state variables $x = [\theta, l_p, p, \phi, Q]^T$ are the controller ($\beta(x)$) inputs. We define as desired interconnection and dissipation matrices:

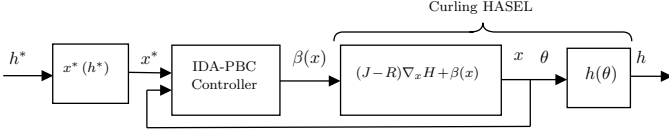


Fig. 6. Closed-loop scheme with the controller $\beta(x)$ inputs are the state variables x and the desired values x^* . The system input is the necessary voltage computed by the controller. $h(x)$ (15) is the function that allows us to find the final position as a function of each link angle.

$$J_d - R_d = \begin{bmatrix} 0 & 0 & J_{13} & 0 & \alpha_1 \\ 0 & 0 & J_{23} & 0 & \alpha_2 \\ -J_{13} & -J_{23} & -r_{33} & J_{43} & \alpha_3 \\ 0 & 0 & -J_{43} & 0 & \alpha_4 \\ -\alpha_1 & -\alpha_2 & -\alpha_3 & -\alpha_4 & -r_{55} \end{bmatrix}, \quad (18)$$

where J_{13} , J_{23} , J_{43} , α_1 , α_2 , α_3 and α_4 are the control design parameters to be determined. The desired closed loop energy function is defined from the desired equilibrium position of the actuator as:

$$H_d = (\theta - \theta^*)^T \tilde{K}_b (\theta - \theta^*) + (l_p - l_p^*)^T \tilde{K} (l_p - l_p^*) + p^T M^{-1} p + (\phi - \phi^*)^T \tilde{K}_\phi (\phi - \phi^*) + (Q - Q^*)^T \tilde{K}_Q (Q - Q^*) \quad (19)$$

The derivative of H_d with respect to x is given by:

$$\nabla_x H_d = \begin{bmatrix} \tilde{K}_b (\theta - \theta^*) \\ \tilde{K} (l_p - l_p^*) \\ M^{-1} p \\ \tilde{K}_\phi (\phi - \phi^*) \\ \tilde{K}_Q (Q - Q^*) \end{bmatrix}. \quad (20)$$

To get the state feedback matching the closed-loop system with a desired PH system $\dot{x} = (J_d - R_d) \nabla_x H_d$ defined above we need to solve the following matching equation:

$$g^\perp [J - R] \nabla_x H = g^\perp [J_d - R_d] \nabla_x H_d, \quad (21)$$

with g^\perp is a full rank annihilator of the input matrix g . We choose the annihilator as follows:

$$g^\perp = \begin{bmatrix} 1 & 0 & 0 & 0 & 0 \\ 0 & 1 & 0 & 0 & 0 \\ 0 & 0 & 1 & 0 & 0 \\ 0 & 0 & 0 & 1 & 0 \end{bmatrix}. \quad (22)$$

We find J_{13} , J_{23} , J_{43} as a function of α_1 , α_2 , α_3 and α_4 .

$$J_{13} = \text{diag}((\text{diag}(M^{-1}p))^{-1}(M^{-1}p - \alpha_1 \tilde{K}_Q(Q - Q^*))); \quad (23)$$

$$J_{23} = \text{diag}((\text{diag}(M^{-1}p))^{-1}(dM^{-1}p - \alpha_2 \tilde{K}_Q(Q - Q^*))); \quad (24)$$

$$r_{33} = \text{diag}((\text{diag}(M^{-1}p))^{-1}(\nabla_\theta H + d\nabla_{l_p} H + bM^{-1}p + \alpha_3 \tilde{K}_Q(Q - Q^*) - J_{13} \tilde{K}_b (\theta - \theta^*) - J_{23} \tilde{K} (l_p - l_p^*) + J_{43} \tilde{K}_\phi (\phi - \phi^*))). \quad (25)$$

$$J_{43} = \text{diag}((\text{diag}(M^{-1}p))^{-1}(r_L L^{-1} \phi - C^{-1}Q + \alpha_4 \tilde{K}_Q(Q - Q^*))); \quad (26)$$

We obtain the control law considering the next design parameters $\alpha_1 = I$, $\alpha_2 = 0$, $\alpha_3 = I$ and $\alpha_4 = 0$.

$$\beta(x) = (\bar{R}ga^T \bar{R}ga)^{-1} \bar{R}ga^T (-\tilde{K}_b (\theta - \theta^*) - M^{-1}p - r_{55} \tilde{K}_Q(Q - Q^*) + L^{-1} \phi + (\bar{R}C^{-1}Q)), \quad (27)$$

Given fixed values for l_p^* and θ^* from the desired endpoint position h^* , we can determine Q^* from the model at steady state.

4.1 Disturbance rejection using Integral Action

In this subsection, we propose to improve the robustness of the controller (27) to two types of disturbances acting on the actuator using a structure-preserving integral action. The first one is the unknown mass load, which can be regarded as the unactuated external force disturbance (d_u). The other one is the disturbance on the actuated input (d_a) i.e. the input voltage. Thus, the disturbed closed-loop system with the previous proposed IDA-PBC control law (27) can be written as:

$$\begin{bmatrix} \dot{Q} \\ \dot{\theta} \\ \dot{l}_p \\ \dot{p} \\ \dot{\phi} \end{bmatrix} = [J_d - R_d] \begin{bmatrix} \nabla_Q H_d \\ \nabla_\theta H_d \\ \nabla_{l_p} H_d \\ \nabla_p H_d \\ \nabla_\phi H_d \end{bmatrix} + \begin{bmatrix} d_a \\ 0 \\ 0 \\ d_u \\ 0 \end{bmatrix}, \quad (28)$$

where the desired interconnection and the damping matrix are defined as:

$$J_d(x) := \begin{bmatrix} J_{aa}(x) & J_{au}(x) \\ -J_{au}^T(x) & J_{uu}(x) \end{bmatrix} = \begin{bmatrix} 0 & -\alpha_1 & -\alpha_2 & -\alpha_3 & -\alpha_4 \\ \alpha_1 & 0 & 0 & -J_{13} & 0 \\ \alpha_2 & 0 & 0 & -J_{23} & 0 \\ \alpha_3 & J_{13} & J_{23} & 0 & -J_{43} \\ \alpha_4 & J_{13} & 0 & J_{43} & 0 \end{bmatrix}; \quad (29)$$

$$R_d(x) := \begin{bmatrix} R_{aa}(x) & R_{au}(x) \\ R_{au}^T(x) & R_{uu}(x) \end{bmatrix} = \begin{bmatrix} r_{55} & 0 & 0 & 0 & 0 \\ 0 & 0 & 0 & 0 & 0 \\ 0 & 0 & 0 & 0 & 0 \\ 0 & 0 & 0 & r_{33} & 0 \\ 0 & 0 & 0 & 0 & 0 \end{bmatrix}. \quad (30)$$

Using the method described in (Ferguson et al., 2017) we choose the new closed-loop Hamiltonian as:

$$H_{cl} = H_d + \frac{K_{int}}{2} (Q - x_c)^2 \quad (31)$$

and the new closed loop system can be derived as:

$$\begin{bmatrix} \dot{x}_a \\ \dot{x}_u \\ \dot{x}_c \end{bmatrix} = (J_{cl} - R_{cl}) \begin{bmatrix} \nabla_{x_a} H_{cl} \\ \nabla_{x_u} H_{cl} \\ \nabla_{x_c} H_{cl} \end{bmatrix} + \begin{bmatrix} d_a \\ 0 \\ 0 \\ d_u \\ 0 \end{bmatrix}. \quad (32)$$

The structure-preserving Integral Action (IA) controller is then given by:

$$\begin{aligned} \dot{x}_c &= -R_{c2}(x) \nabla_{x_a} H + (J_{au} + R_{au}) \nabla_{x_u} H, \\ u_{int} &= [-J_{aa} + R_{aa} + J_{c1}(x) - R_{c1}(x) - R_{c2}(x)] \nabla_{x_a} H + [J_{c1}(x) - R_{c1}(x)] K_{int} (x_a - x_c) + 2R_{au} \nabla_{x_u} H; \end{aligned} \quad (33)$$

where u_{int} is the output of the IA controller. x_c is the IA controller state. The actuated state is the charge Q_m whilst the unactuated states are the angle θ , the length l_p , the angular momentum p , and the magnetic flux ϕ .

From $J_{au} = -[\alpha_1 \ 0 \ \alpha_3 \ 0]$, $J_{c1} = R_{c2} = R_{au} = 0$ and $R_{c1} = r_{55}$ we obtain the control law:

$$\begin{aligned} u_{int} &= -r_{55} K_{int} (Q - x_c); \\ \dot{x}_c &= -(\alpha_1 \tilde{K}_b (\theta - \theta^*) + \alpha_3 M^{-1} p). \end{aligned} \quad (34)$$

where the design parameter K_{int} is chosen as a vector of dimensions $1 \times n$. The dimension of the controller $\beta(x)$

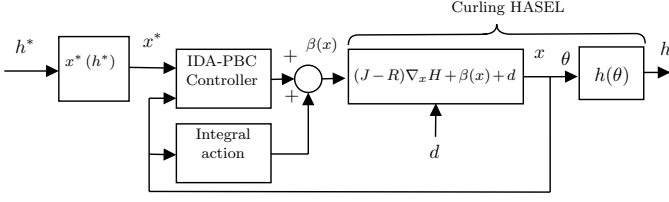


Fig. 7. Closed-loop scheme with IA.

is 1×1 . The control scheme is shown in Fig. 7 and the interconnection and damping matrix are given by:

$$J_{cl} := \begin{bmatrix} 0 & J_{au} & 0 \\ -J_{au}^T & J_{uu} & 0 \\ 0 & 0 & 0 \end{bmatrix}; \quad R_{cl} := \begin{bmatrix} r_{55} & 0 & r_{55} \\ 0 & r_{33} & 0 \\ r_{55} & 0 & r_{55} \end{bmatrix}. \quad (35)$$

5. NUMERICAL SIMULATION

In this section, we validate the proposed control methods with numerical simulations. The parameters of the actuator are given in Table. 1. We implement the IDA-PBC controller (27) with the Integral action controller (34) to achieve the desired endpoint position of the curling actuator. To show the different closed loop dynamics performances, we vary the tuning parameter \tilde{K}_b while keeping the rest of the tuning parameters constant. The controller parameters values are $r_{55} = \text{diag}([0.1 \ 0.1 \ 0.1 \ 0.1])$ and $\tilde{K}_{int} = [0.5 \ 11 \ 1.2 \ 0.5]$. One can observe the endpoint regulation to the desired position in Fig. 8 using the IDA-PBC method and the rejection of external disturbances in Fig. 9 with the IDA-PBC+IA method.

Fig. 8 represents the actuator displacement when \tilde{K}_b is tuned, while the parameter \tilde{K}_Q is fixed to a constant value. The desired endpoint position is $h^*(\theta) = 2$ cm. From simulation results shown in Fig. 8, the response time of the closed-loop system decreases when \tilde{K}_b increases, since \tilde{K}_b can be seen as the actuator's stiffness in the closed-loop system.

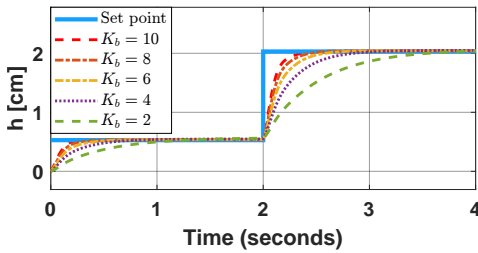
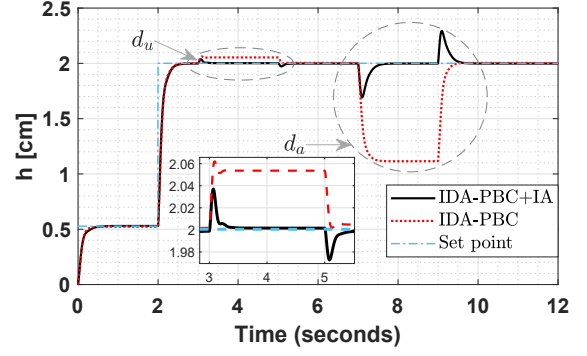
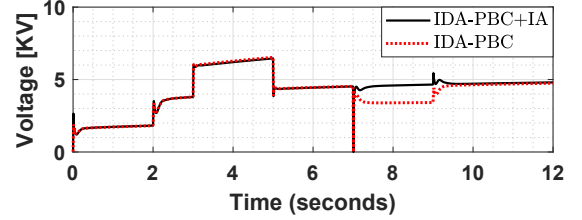


Fig. 8. Position control keeping constant the parameters $\tilde{K}_Q = 1000$, the set-point equal to 2cm and varying the tuning parameter related with the desired angle \tilde{K}_b .

Fig. 9 shows the actuator displacement to different desired set points. The external unactuated disturbance $d_u = -0.04\text{Nm}$ is added at 3s during 2s, and the actuated disturbance $d_a = -30\text{V}$ is added at 7s during 2s (0.3% of full scale according to the amplifier specifications). The proposed controller with IA can reject the disturbances, while the controller without IA can not reject these disturbances. From the simulation results shown in Fig. 9(b), it is seen that the applied controlled voltage on the closed



(a)



(b)

Fig. 9. (9a) Position control $\tilde{K}_Q = 1000$, $\tilde{K}_b = 10$ and $\tilde{K}_{int} = [0.5 \ 11 \ 1.2 \ 0.5]$. The simulation presents disturbances d_u and d_a at 3s and 7s respectively. (9b) IDA-PBC and IDA-PBC+IA control signals.

loop actuator always remains below 10kV, which aligns with the physical consistency of the experimental setup.

6. CONCLUSION

In this paper we use the port-Hamiltonian framework to model and control a curling HASEL actuator. The actuator's dynamics is divided into two components. The mechanical part of the actuator is characterized by linear and torsional springs, while the deformable capacitor and the inductor represent the electrical part of the system, the coupling being done through the conservation of volume of the overall system. This model can cope with the main dynamic behavior of the actuator with nonlinearities such as the drift effect. An IDA-PBC controller with the integral action is proposed to control the position of the actuator. It is shown that the actuator endpoint position follows the set point and that we can adjust the dynamic performances by varying the tuning parameters of the controller. The use of integral action has improved the robustness of the closed-loop system against external disturbances.

The perspectives of this work are to implement and validate the proposed IDA-PBC controller with IA in the experimental setup. Furthermore, we intend to model and control more complex structures and soft robots based on HASEL actuators (e.g., scorpion, fish, human hands-inspired designs) with the interconnection of basic subsystems.

REFERENCES

- Acome, E., Mitchell, S.K., Morrissey, T.G., Emmett, M.B., Benjamin, C., King, M., Radakovitz, M., and Keplinger, C. (2018). Hydraulically amplified self-healing electrostatic actuators with muscle-like performance. *Science*, 359(6371), 61–65.

- Ayala, E.P., Wu, Y., Rabenoroso, K., and Le Gorrec, Y. (2022). Energy-based modeling and control of a piezotube actuated optical fiber. *IEEE/ASME Transactions on Mechatronics*, 1–11.
- Ferguson, J., Donaire, A., Ortega, R., and Middleton, R.H. (2017). New results on disturbance rejection for energy-shaping controlled port-Hamiltonian systems.
- Franco, E., Casanovas, A.G., Tang, J., y Baena, F.R., and Astolfi, A. (2021a). Position regulation in cartesian space of a class of inextensible soft continuum manipulators with pneumatic actuation. *Mechatronics*, 76, 102573.
- Franco, E., Garriga-Casanovas, A., Tang, J., y Baena, F.R., and Astolfi, A. (2021b). Adaptive energy shaping control of a class of nonlinear soft continuum manipulators. *IEEE/ASME Transactions on Mechatronics*, 27(1), 280–291.
- Hainsworth, T., Schmidt, I., Sundaram, V., Whiting, G.L., Keplinger, C., and MacCurdy, R. (2022). Simulating electrohydraulic soft actuator assemblies via reduced order modeling. In *2022 IEEE 5th International Conference on Soft Robotics (RoboSoft)*, 21–28. IEEE.
- Kellaris, N., Rothmund, P., Zeng, Y., Mitchell, S.K., Smith, G.M., Jayaram, K., and Keplinger, C. (2021). Spider-inspired electrohydraulic actuators for fast, soft-actuated joints. *Advanced Science*, 8(14), 2100916.
- Kim, S. and Cha, Y. (2021). Double-layered electrohydraulic actuator for bi-directional bending motion of soft gripper. In *2021 18th International Conference on Ubiquitous Robots (UR)*, 645–649.
- Ly, K., Mayekar, J.V., Aguasvivas, S., Keplinger, C., Rentschler, M.E., and Correll, N. (2022). Electro-hydraulic rolling soft wheel: Design, hybrid dynamic modeling, and model predictive control. *IEEE Transactions on Robotics*.
- Ortega, R., van Der Schaft, A., Maschke, B., and Escobar, G. (2002). Interconnection and damping assignment passivity-based control of port-controlled Hamiltonian systems. *Automatica*, 38(4), 585–596.
- Rothmund, P., Kellaris, N., Mitchell, S.K., Acome, E., and Keplinger, C. (2021). HASEL artificial muscles for a new generation of lifelike robots—recent progress and future opportunities. *Advanced Materials*, 33(19), 2003375.
- Tian, Y., Liu, J., Wu, W., Liang, X., Pan, M., Bowen, C., Jiang, Y., Sun, J., McNally, T., Wu, D., et al. (2022). Peano-hydraulically amplified self-healing electrostatic actuators based on a novel bilayer polymer shell for enhanced strain, load, and rotary motion. *Advanced Intelligent Systems*, 2100239.
- van der Schaft, A. (2000). *L2-gain and passivity techniques in nonlinear control*. Springer.
- Volchko, A., Mitchell, S.K., Morrissey, T.G., and Humbert, J.S. (2022). Model-based data-driven system identification and controller synthesis framework for precise control of siso and miso HASEL-powered robotic systems. In *2022 IEEE 5th International Conference on Soft Robotics (RoboSoft)*, 209–216. IEEE.
- Yeh, Y., Cisneros, N., Wu, Y., Rabenoroso, K., and Gorrec, Y.L. (2022). Modeling and position control of the HASEL actuator via port-Hamiltonian approach. *IEEE Robotics and Automation Letters*, 7(3), 7100–7107.